The Eurasia Proceedings of Science, Technology, Engineering & Mathematics (EPSTEM)
ISSN: 2602-3199

The Eurasia Proceedings of Science, Technology, Engineering and Mathematics (EPSTEM), 2025

Volume 38, Pages 423-432

IConTES 2025: International Conference on Technology, Engineering and Science

Synthesis and Characterization of Biochar and Nano-Biochar Composites Derived from Biomass (*Colutea cilicica*) for the Removal of Cationic Dyes from Aqueous Solutions

Erol Pehlivan
Konya Technical University

Busra Ozkok
Konya Technical University

Abstract: In this study, the removal of Methylene blue (MB) and Malachite green (MG) dyestuffs from aqueous solutions was investigated using biochar and iron-modified biochar derived from biomass (*Colutea cilicica*). Biochar was prepared by pyrolyzing biomass at 500 °C with a heating rate of 10 °C/min, and further modified with nanoscale zero-valent iron (nZVI) to obtain nZVI-biochar. The adsorption performance of both biochar and nZVI-biochar was systematically evaluated under varying experimental conditions, including solution pH, contact time, adsorbent dosage, and initial dye concentration. Equilibrium and kinetic studies were performed, along with thermodynamic analyses at different temperatures. The optimum pH for dye removal was determined as 7.0. Adsorption equilibrium was reached within 120 min, and the kinetic data were best described by the pseudo-second-order model. Equilibrium data fitted well to the Langmuir isotherm model. The maximum adsorption capacities were 70.67 mg/g (biochar) and 81.17 mg/g (nZVI-biochar) for MB, and 61.43 mg/g (biochar) and 83.13 mg/g (nZVI-biochar) for MG. Overall, the modified nZVI-biochar composite exhibited significantly enhanced adsorption capacity compared to unmodified biochar. The synthesized nano-biochar composite can be proposed as a potential alternative adsorbent for the removal of cationic dyes from wastewater.

Keywords: Adsorption, Biomass, Biochar, Nano-iron composite, Cationic dyes

Introduction

Water pollution, a major contributor to overall environmental degradation, remains one of the most pressing global challenges of the modern era. While technological advancements enhance human comfort and industrial efficiency, they also intensify the rate at which natural ecosystems are disrupted. In light of the accelerating decline in clean and accessible freshwater resources and the increasing likelihood of severe scarcity in the near future the development and optimization of wastewater treatment and recovery technologies have become imperative. During the natural hydrological cycle, the introduction of pollutants from diverse anthropogenic and natural origins results in substantial degradation of water quality, thereby posing serious risks to human health, ecological integrity, and long-term environmental sustainability (Rathi et al., 2021; Erkmen et al., 2019).

One significant form of industrial pollution is dye contamination, which arises predominantly from the operations of the textile and dyeing industries. Owing to the continuous expansion of these sectors, large quantities of synthetic dyes are regularly introduced into the water, contributing to increasing levels of dye-laden effluents in aquatic environments. Due to factors such as the increasing diversity of dyes and the large volumes of dye-laden water used and subsequently discharged during textile dyeing processes, these effluents are classified as high-priority wastewater streams requiring immediate and effective treatment. Water containing dye pollution prevents the sun's rays from reaching the environment by giving color to the receiving environments, which gives negative

ecological consequences (Yaseen & Scholz, 2019; Erkuş et al, 2018). Adsorption, which is among the advanced treatment methods, has been preferred recently. Adjustable process conditions and high treatment efficiency provide advantages. However, scientists have focused on the search for an economical adsorbent in recent years due to the high volume of wastewater that needs to be treated and the costs of adsorbents. A critical point to be considered is that the adsorbent to be used not only cleans wastewater but also does not contain toxic chemicals. Biomasses, which are environmentally friendly, easily available and economical materials, stand out as a potential adsorbent (Parlayıcı & Pehlivan, 2021).

Biomass is a broad term encompassing all non-fossilized biological materials derived from living organisms. Typical biomass sources include plant components such as seeds, roots, leaves, and tree bark, as well as agricultural residues and various forms of animal waste. However, literature reports consistently show that the adsorption performance of untreated (raw) biomass is often inadequate for the efficient removal of toxic dyes from aqueous systems. As a result, numerous studies have focused on improving its adsorption capacity through additional processing techniques. These enhancement approaches frequently involve surface modification or chemical activation of the biomass, which serve to increase its surface area, introduce functional groups, and improve its overall structural properties, thereby enhancing its interaction with dye molecules (Erdogan, 2017).

Biochar, essentially a carbon-rich material derived from biological sources, has emerged as a promising adsorbent for wastewater treatment. Its applicability in this field has gained significant research attention in recent years. Owing to their inherently large surface area and highly porous architecture, biochars exhibit advantageous properties for surface-driven processes such as adsorption. Indeed, numerous studies have demonstrated the successful removal of toxic dyes from wastewater using biochar-based adsorbents (Baig et al., 2014; Parlayıcı & Pehlivan, 2023). Despite their potential for capturing dye molecules from aqueous media, biochar-based adsorbents also present certain limitations. Over time, pore blockage and the depletion of available functional groups capable of binding pollutants may hinder complete dye removal. One effective strategy to overcome these efficiency challenges is the incorporation of nanoparticles into biochar matrices to synthesize advanced composite adsorbents.

In this study, the seeds of *Colutea cilicica* were utilized as the raw biomass precursor. The synthesized biochar was subsequently modified with iron nano-particles. Equilibrium and thermodynamic investigations were conducted to evaluate the removal of MB and MG dyes from aqueous solutions, during which the effects of key adsorption parameters including pH, contact time, adsorbent dosage, and initial dye concentration were systematically examined to determine the optimal operating conditions. Experimental data were analyzed using the Langmuir, Freundlich, and Temkin isotherm models. Kinetic studies were performed to elucidate the influence of contact time on the adsorption process. Furthermore, temperature-dependent dye removal experiments enabled the calculation of Gibbs free energy, enthalpy, and entropy values, thereby facilitating the identification of the most favorable operational temperature. Overall, the findings demonstrate that both the pristine and modified biochars are efficient adsorbents for the removal of dyes from aqueous media.

Results and Discussion

Materials and Experimentation

Iron (III) chloride hexahydrate, iron(II) sulfate heptahydrate, and ammonia (NH_3) were supplied by Merck. Methylene Blue (MB) and Malachite Green (MG) dyes were obtained from Acros Organics (New Jersey, USA). All chemicals used in the experiments were of analytical grade. *Colutea cilicica* tree seeds (Turkish “Patlangaç” tree seeds were collected from a field near Konya, Türkiye, and utilized as the biomass source for adsorbent synthesis. For biochar preparation, a Magma Therm MT1210-B2 muffle furnace was used, and a Biosan PSU-10 orbital shaker and a glass-electrode pH meter (Apera Instruments pH700) were employed during the experiments. The concentrations of MB and MG were determined using a UV–visible spectrophotometer (Shimadzu UV-1700). FT-IR spectra were recorded using a Thermo Scientific Nicolet iS20 spectrometer, while XRD analysis was performed using a Europe model X-ray diffractometer. The microstructure of the adsorbent was examined with a scanning electron microscope (SEM, Zeiss Gemini SEM 500).

Preparation of Raw Material and Biochar

*Colutea cilic*ica seeds were cleaned to remove surface impurities, thoroughly washed, and subsequently dried. The dried seeds were ground into a fine powder using a laboratory mill. The resulting powder was washed several

times with 0.1 mol L^{-1} HCl, followed by repeated washing with distilled water, and then dried at room temperature for 24 h. The prepared biomass was converted into biochar through slow pyrolysis in a custom-designed stainless-steel reactor with a sealed steel lid, placed inside a muffle furnace. Pyrolysis was conducted under limited oxygen conditions and a nitrogen atmosphere at 400–500 °C for 3 h, with a controlled heating rate of 10 °C min^{-1}. After pyrolysis, the sample was cooled to room temperature and washed with 0.1 M HCl, followed by repeated rinsing with ultrapure water until a stable pH was achieved. The obtained *Colutea cilicica* biochar was oven-dried, ground using a laboratory grinder, and sieved to obtain uniform particle sizes (150–200 µm). The resulting biochar fraction was then used for composite synthesis.

Synthesis of Adsorbent

The preparation procedure for zero-valent iron *Colutea cilicica* biochar (nZVI-biochar) is illustrated in Figure 1. The nZVI-biochar composites were synthesized via a simple chemical co-precipitation method. For this purpose, 5 g of biochar adsorbent was weighed and transferred into a batch reactor vessel. Subsequently, 6 g of $FeCl_3 \cdot 6H_2O$ and 4 g of $FeSO_4 \cdot 7H_2O$ were added, followed by the addition of 50 mL of ultrapure water. The mixture was stirred using an orbital shaker to obtain a homogeneous suspension. The pH of the reaction medium was adjusted to 10 by the dropwise addition of 1 M NH_4OH. The reaction was maintained at 50 °C under continuous stirring for 1 h. The resulting nano-Fe^0 loaded biochar was filtered through filter paper and washed several times with ultrapure water to remove residual impurities. The synthesized biochar composite was dried in an oven at 40 °C for 24 h, repeatedly rinsed with deionized water, and then allowed to dry for an additional 24 h before being stored for further use.

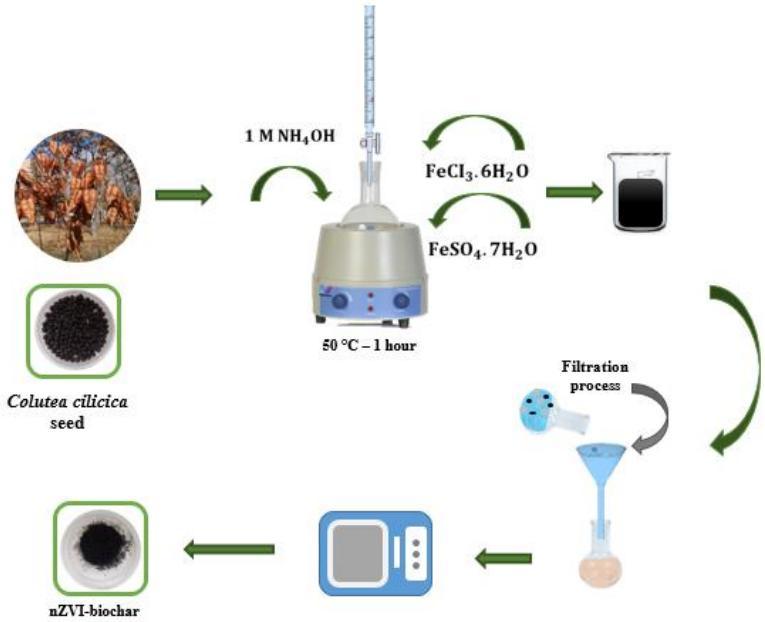

Figure 1. Schematic steps of nZVI-biochar synthesis

Batch Adsorption Experiments

Adsorption experiments for MB and MG were initially conducted using 25 ppm MB and 50 ppm MG solutions, respectively. To evaluate the influence of various parameters on the adsorption efficiency and capacity of biochar and nZVI-biochar composites, a series of systematic batch experiments were performed in beakers at 25 °C. The parameters optimized included solution pH (2, 3, 4, 5, 6, 7, 8, and 9), initial dye concentration (15, 25, 50, 75, 100, and 125 mg L^{-1}), adsorbent dosage (0.001, 0.003, 0.005, 0.01, 0.015, and 0.02 g L^{-1}), contact time (20, 30, 45, 60, 90, 120, 150, 180, and 240 min), and temperature (25, 35, and 45 °C). To ensure the accuracy, reliability, and reproducibility of the experimental findings, all samples were analyzed in duplicate. For comparison of adsorption performance, both the composite material and pristine biochar were tested under identical conditions using standard MB and MG solutions. Following the adsorption process, the residual dye concentration in the filtrate was determined at regular intervals using UV–Vis spectrophotometry. Finally, adsorption capacity (q_e, mg g^{-1}) and removal efficiency (%) were calculated based on the differences between initial and final dye concentrations.

The concentrations of MG and MB in the filtrate were determined using a UV–Vis spectrophotometer (λ = 617 nm for MG and λ = 664 nm for MB). The percentage adsorption of MB and MG was calculated using Equations (1) and (2):

$$q_e = \frac{(C_o - C_e)V}{m} \quad (1)$$

$$Removal(\%) = \frac{(C_o - C_e)100}{C_o} \quad (2)$$

Structural and Morphological Characterization of the Nano-Composites and Biochar

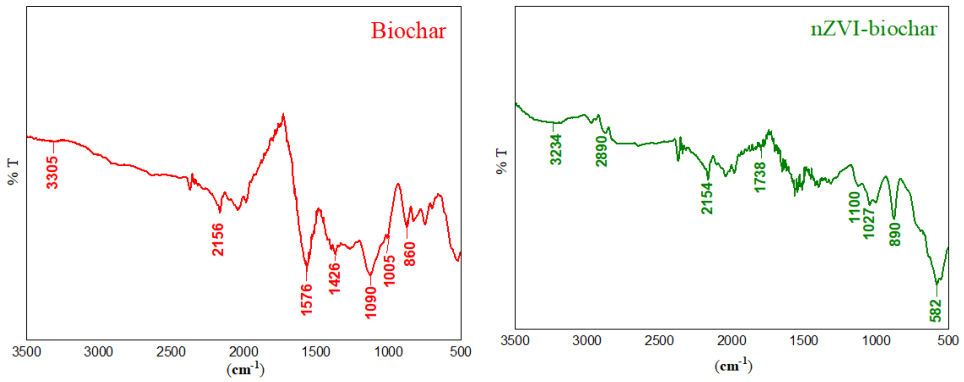

(a) (b)

Figure 2. FT-IR diagram of biochar (a), nZVI-biochar (b)

Figure 2(a–b) presents the FT-IR spectra of the biochar and nZVI-biochar composites. The peaks observed around 1741 cm^{-1} in both biochar and nZVI-biochar correspond to the stretching vibrations of C=O bonds. The characteristic Fe–O vibration band appearing at 582 cm^{-1} is attributed to iron oxides, indirectly confirming the successful synthesis of magnetic biochar (Yi et al., 2020). In the nZVI-biochar adsorbent, the peak at 582 cm^{-1} further verifies the presence of iron components, while the peak at 890 cm^{-1} corresponds to the fingerprint region. In biochar, the peaks near 1600 cm^{-1} are associated with aromatic C=O ring stretching attributed to similar phytochemical components, whereas those around 1430 cm^{-1} likely arise from aromatic C–O ring stretching. The peak at 1090 cm^{-1} in biochar is assigned to C–O stretching vibrations. The peak at 2155 cm^{-1} in biochar, along with the peaks at 2154 cm^{-1} and 2890 cm^{-1} in nZVI-biochar, corresponds to the C≡C stretching of alkyne groups. Additionally, the peaks between 1027 and 1100 cm^{-1} in nZVI-biochar are attributed to the vibrational modes of C–O–C and C–O functional groups (Parlayıcı & Pehlivan, 2017). Overall, the FT-IR characterization results indicate that the waste biomass-derived biochars possess a wide variety of functional groups capable of participating in the biosorption of cationic dyes from aqueous media. The presence of numerous organic active groups (such as –OH, –CO, –COOH, C=O, and –CH) significantly contributes to the adsorption of dye molecules.

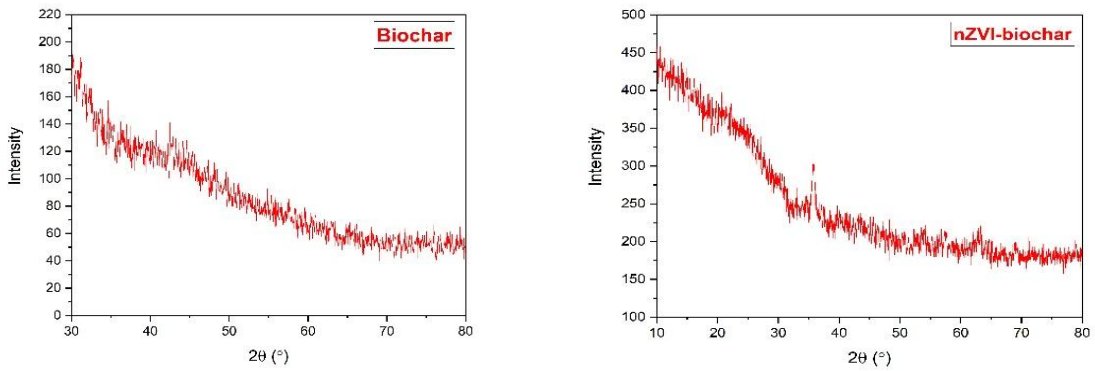

Figure 3. XRD diagram of biochar (a), nZVI-biochar (b)

Figure 3(a–b) shows the XRD patterns of the biochar and nZVI-biochar composites. In the biochar diffractogram, the peaks at 2θ = 47.5° and 64.9° correspond to CaO, while the peaks at 2θ = 43.1° and 57.0° indicate the presence of $CaCO_3$ (Hung et al., 2021). The nZVI-biochar nanocomposite exhibits characteristic diffraction peaks at 2θ =

30.2°, 35.5°, 43.2°, 53.7°, 57.2°, 62.7°, and 74.3°. These peaks are attributed to Fe_3O_4, confirming that magnetite is the dominant crystalline phase and that Fe_3O_4 was successfully loaded onto the adsorbent surface (Parlayıcı & Pehlivan, 2023). The broad peak observed at $2\theta = 24°$ for biochar represents the typical diffraction pattern of amorphous carbon.

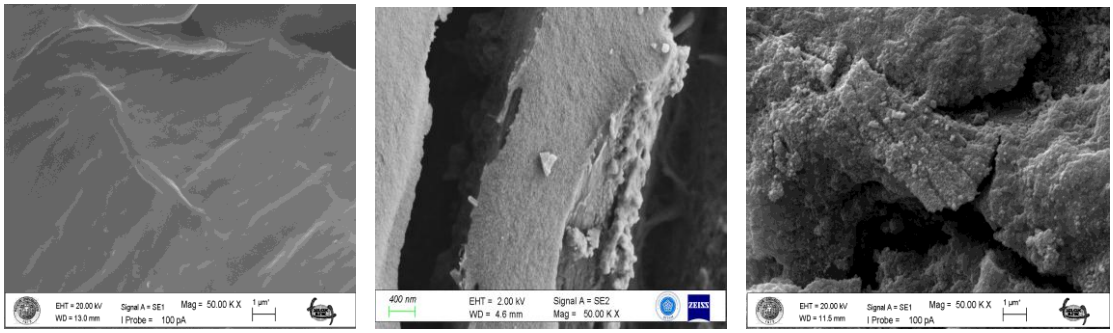

(a) (b) (c)

Figure 4. SEM image of seed (a) biochar (b) nZVI-biochar (c)

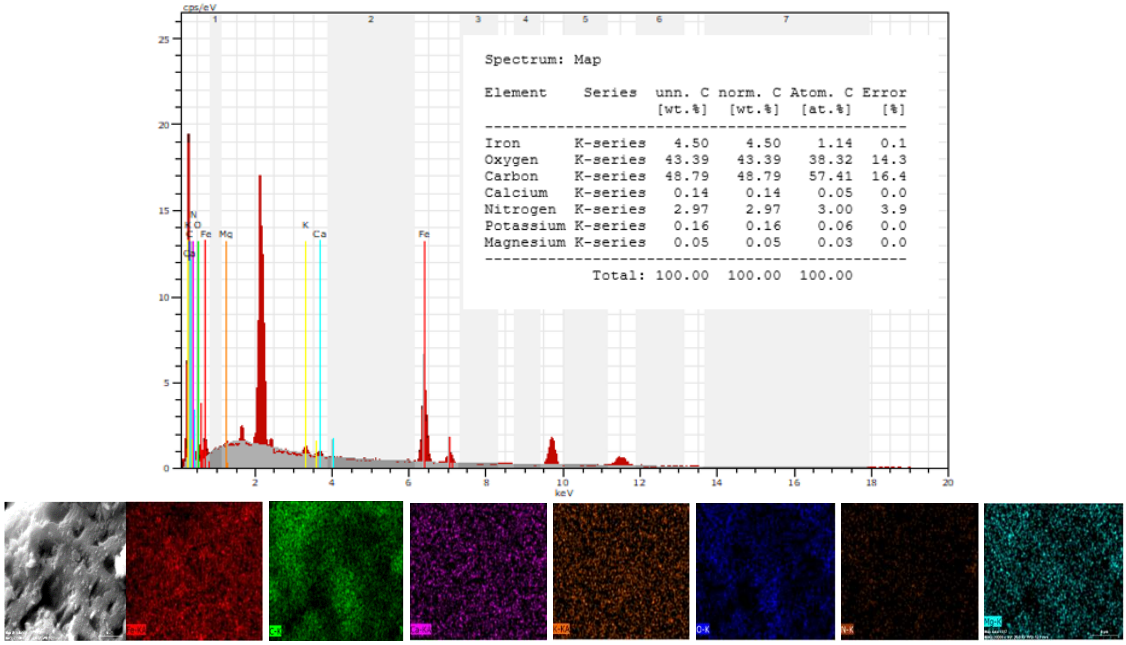

Figure 5. EDX image nZVI-biochar

The morphological characteristics and elemental composition of the seed, biochar, and nZVI-biochar composites were examined using scanning electron microscopy (SEM) (Figure 4) and energy-dispersive X-ray spectroscopy (EDX) (Figure 5). The raw seed biomass exhibited smooth, compact layers with limited porosity (Figure 4a). Since porous structures provide a greater number of active adsorption sites, higher porosity is desirable for efficient dye adsorption. After pyrolysis, the biochar biomass developed noticeable pores due to the release of volatile components and structural changes in its lignin content (Figure 4b). As a result, more pronounced pores and voids were observed in the biochar adsorbent produced via the pyrolysis process. The nZVI-biochar surface exhibited irregular folds and non-uniformly distributed pores (Figure 4c). As shown in Figure 5, EDX analysis confirmed the successful incorporation of iron into the structure of the nZVI-biochar nanocomposite. The adsorbent structure also displayed high relative abundances of oxygen and carbon, with the percentage of each detected element presented in the analysis output. The elemental composition of the nanocomposite is shown as percentage distributions in the EDX spectrum.

Results of the Batch Adsorption Experiments

Effect of Biochar and nZVI-Biochar Dosage

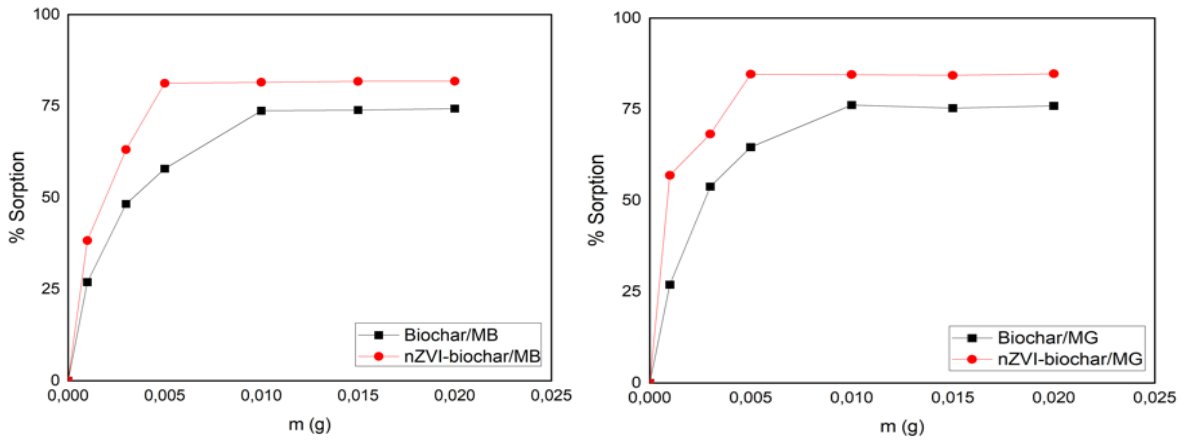

Figure 6. Effect of biochar and nZVI-biochar composite dosage

The dye uptake was investigated at different adsorbent dosages (0.001, 0.003, 0.005, 0.01, 0.015, and 0.02 g L^{-1}) through adsorption experiments. Figure 6 presents the percentage sorption as a function of the varying adsorbent dosages. In general, the adsorption capacity of the adsorbent increases with increasing dosage up to a certain point, after which it levels off. At longer contact times, only minor changes in the percentage adsorption were observed with further increases in adsorbent amount. For both MG and MB dyes, the adsorption capacity increased proportionally with the adsorbent dosage up to 0.010 g L^{-1}.

Effect of pH

To investigate the effect of pH on dye adsorption, the initial pH of the dye solutions was adjusted from 2.0 to 9.0. pH values above 9 were not examined because the highly basic conditions reduce dye adsorption. Changes in solution pH significantly influence dye biosorption by affecting the active adsorption sites on the biosorbent surface and the surface charge profile of the biosorbent. For an anionic dye, an increase in H^+ ion concentration renders the adsorbent surface positively charged, enhancing electrostatic attraction and promoting dye uptake. In contrast, for cationic dyes MG and MV, a pH greater than 4 is preferred, as higher pH values increase the concentration of OH^- ions, resulting in a negatively charged adsorbent surface. This enhances the electrostatic interaction between the positively charged cationic dye and the negatively charged biochar surface, thereby increasing dye absorption. The surface layers of biochar and nZVI-biochar generate an electric charge effect for MG and MB, facilitating dye attachment to the biosorbent surface. Consequently, the electrostatic attraction between positively charged cationic dyes and the negatively charged biochar surface is enhanced, improving adsorption efficiency (Srivatsav et al., 2020). The variations in biosorption capacities of MG and MB under different solution pH conditions are presented in Figure 7.

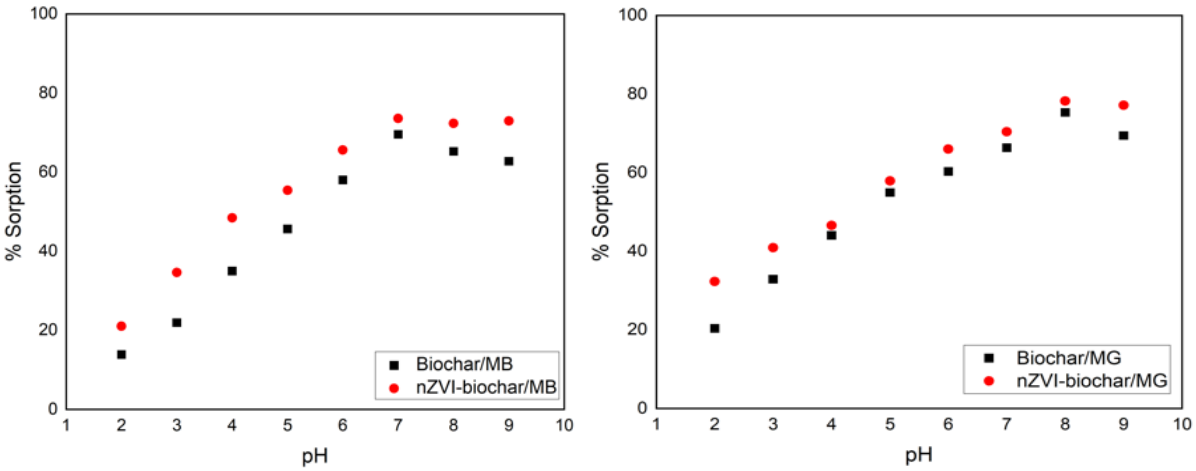

Figure 7. The effect of pH on dye adsorption.

Effect of Dye Initial Concentration

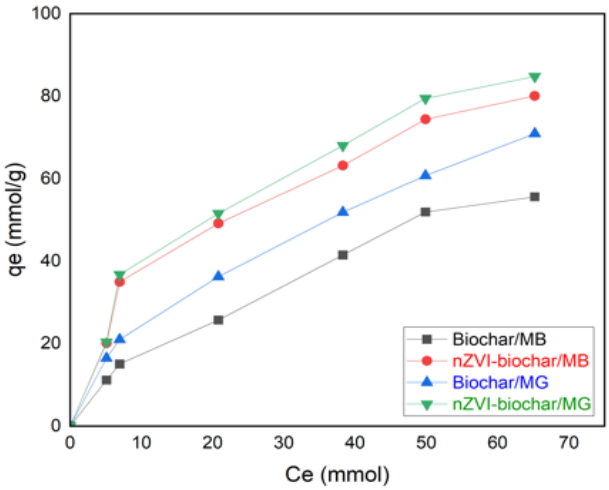

Figure 8. Effect of dye concentration

The adsorption isotherms for dye removal using the biochar and nanocomposite are presented in Figure 8. The graph, which plots the amount of adsorbed dye (q_e) against the equilibrium concentration (C_e), represents a typical single-layer adsorption process. Adsorption capacity was evaluated by varying the initial dye concentration (15, 25, 50, 75, 100, and 125 ppm). As the initial dye concentration increased, the difference in adsorption capacity between the biochar and the nanocomposite became more pronounced. Initially, the amount of adsorbed dye increased rapidly with rising dye concentration. At higher concentrations, the functional groups on the biochar and nanocomposite became saturated, and the adsorption potential reached equilibrium, at which point no further interaction occurred.

For equilibrium analysis, the Langmuir, Freundlich, and Temkin isotherm models were applied (Table 1). The Freundlich model represents physical adsorption at equilibrium, indicating that the biosorbent surface is heterogeneous and covered with MG and MB molecules. The Freundlich constants, K_f and n, were calculated; when n lies between 1 and 10, dye biosorption is considered favorable. The Langmuir isotherm represents chemical, monolayer adsorption and is widely recognized as the simplest theoretical model for single-layer biosorption. Magnetic modification of the raw material enhanced the adsorption capacities of the biosorbents. The results from the equilibrium studies suggest that both MG and MB can be efficiently removed from aqueous solutions. For biochar and nZVI-biochar, Langmuir correlation coefficients (R^2) exceeded 0.99 (Table 1), indicating that the Langmuir model best describes the adsorption process compared with other isotherms. The dimensionless separation factor (R_L) further confirms adsorption favorability: values between 0 and 1 indicate suitable biosorption, while $R_L > 1$ suggests otherwise. In this study, all R_L values (Table 1) ranged between 0 and 1, demonstrating strong adsorption of MG and MB from solution by the adsorbents. According to the Temkin isotherm, the positive B_T values indicate that the adsorption heat capacity increases with rising temperature, suggesting endothermic adsorption (Gozeten & Savran, 2018).

Table 1. Adsorption isotherm parameters for removal of dye.

Model	**Adsorbents**	**Dye**	**Parameters for dye**			
			A_s	**K_b**	**R^2**	**R_L**
Langmuir	Biochar	MB	70.671	0.037	0.993	0.519
$\frac{C_e}{q_e} = \frac{C_e}{A_s} + \frac{1}{K_b A_s}$	Biochar	MG	61.425	0.202	0.995	0.090
	nZVIbiochar	MB	81.169	0.076	0.978	0.207
	nZVIbiochar	MG	83.126	0.101	0.980	0.165
			K_F	**n**	**R^2**	
Freundlich	Biochar	MB	4.140	1.59	0.980	
$Inq_e = 1nK_f + \frac{1}{n}1nC_e$	Biochar	MG	13.208	2.38	0.990	
	nZVIbiochar	MB	11.914	2.34	0.957	
	nZVIbiochar	MG	11.442	2.00	0.947	
			B_T	**A_T**	**R^2**	
Temkin	Biochar	MB	17.431	0.321	0.940	
$q_e = B_T \ln A_T + B_T \ln c_e$	Biochar	MG	15.305	1.367	0.964	
	nZVIbiochar	MB	19.064	0.621	0.980	
	nZVIbiochar	MG	22.632	0.615	0.939	

Effect of Contact Time and Kinetic Studies

In adsorption studies, the contact time of the biosorbent plays a critical role. The effect of contact time on the biosorption of MG and MB is shown in Figure 9. For this purpose, 25 ppm MB and 50 ppm MG solutions were individually added to 0.01 g L^{-1} of biochar and nZVI-biochar adsorbents. The resulting suspensions were stirred using a magnetic stirrer for predetermined time intervals (20, 30, 45, 60, 90, 120, 150, 180, and 240 minutes) and subsequently filtered. The residual concentrations of MG and MB in the filtrate were determined using UV–Vis spectrophotometry.

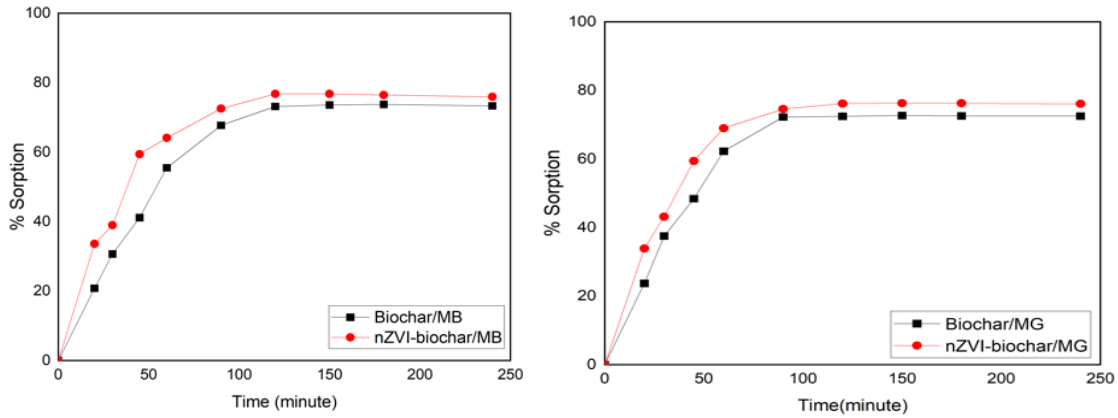

Figure 9. Influence of contact time on adsorption.

As illustrated in Figure 9, the biosorption of MG and MB by the adsorbents increased rapidly during the initial 0–45 minutes. After 45 minutes, the adsorption rate slowed, and equilibrium was achieved at longer contact times. Factors influencing the time required to reach equilibrium include the structural characteristics of the adsorbent, environmental conditions, and the molecular properties of the dyes. Consequently, the equilibrium attainment times varied between the different adsorbents.

Kinetic Models for Equlibrium

Pseudo-first-order and pseudo-second-order kinetic models were applied to investigate the biosorption of MG and MB onto biochar and nZVI-biochar, and the kinetics were analyzed. The calculated kinetic parameters for both dyes are presented in Table 2. The pseudo-first-order model was found to be applicable for MG and MB adsorption on both the raw and magnetite-modified biosorbents. However, for both adsorbents, the equilibrium adsorption capacity (q_e) calculated from the pseudo-second-order model showed smaller deviations from the experimental data than that obtained from the pseudo-first-order model. Therefore, the pseudo-second-order kinetic model was determined to better describe the biosorption mechanism of the system.

Table 2. Comparison of the pseudo-first-order, pseudo-second-order adsorption rate constants and calculated and experimental q_e values obtained at different initial dye concentrations.

				Pseudo-first-order			**Pseudo-second-order**		
Adsorbents	**Dye**	**C_o(ppm)**	**q_e exp**	**k_1**	**q_e**	**R^2**	**k_2**	**q_e**	**R^2**
Biochar	MB	**25**	15.054	0.016	15.06	0.843	0.0008	22.49	0.961
Biochar	MG	**50**	36.255	0.013	36.26	0.897	0.0007	40.30	0.973
nZVIbiochar	MB	**25**	20.136	0.017	20.14	0.860	0.0016	19.28	0.971
nZVIbiochar	MG	**50**	40.994	0.011	41.00	0.821	0.0012	39.98	0.990

Thermodynamic Studies

The thermodynamic parameters for the biosorption of dyes onto the biosorbents, including ΔH° (J mol^{-1}), ΔS° (J K^{-1} mol^{-1}), and ΔG° (J mol^{-1}), are presented in Table 3. It was observed that both the adsorption capacity and the percentage removal of the dyes by the biochar and nanocomposite increased with rising temperature. The negative values of ΔG° indicate the feasibility of the adsorption process and confirm that dye adsorption occurs spontaneously. Adsorption was more favorable at lower temperatures (298 K). Positive ΔH° values suggest that

the interaction between the dyes and the adsorbents is endothermic. Additionally, the positive ΔS° values indicate an increase in randomness at the solid–solution interface during dye adsorption (Gözeten & Savran, 2018).

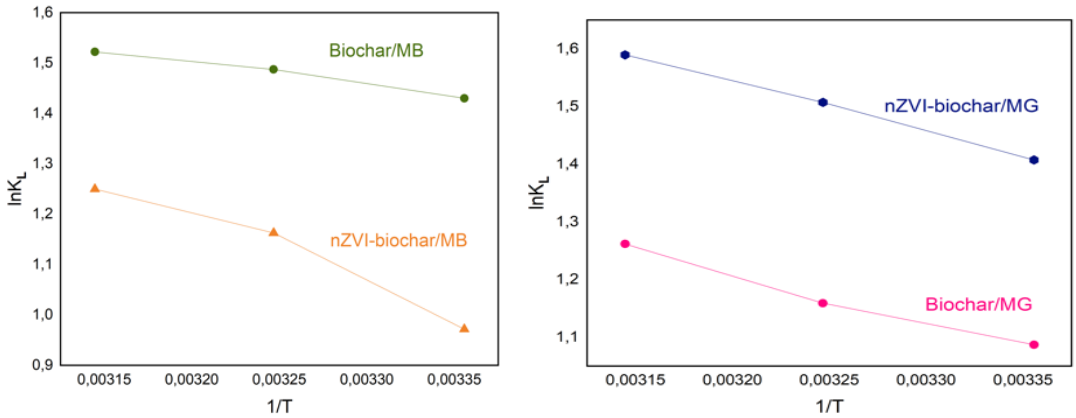

Figure 10. The impact of temperature on dye adsorption.

Table 3. Thermodynamic parameters for adsorption of dye

		ΔS°	**ΔH°**	**ΔG°**				
				T=298.15K	T=308.15K	T=318.15K	T=328.15K	R^2
Biochar	MB	24.12	3637.87	-3543.16	-3808.78	-4024.55	-4024.55	0.970
Biochar	MG	32.04	6870.04	-2693.04	-2967.67	-3335.90	-3335.90	0.971
nZVIbiochar	MB	45.10	10995.78	-2407.77	-2977.54	-3304.63	-3304.63	0.926
nZVIbiochar	MG	35.81	7181.67	-3486.87	-3859.35	-3859.35	-4202.56	0.997

Conclusion

The results of this study demonstrate that both the biochar and the nanocomposite are sustainable and highly efficient biosorbents for dye removal from aqueous systems. The adsorption capacities were determined as 70.67 mg g^{-1} (biochar) and 81.17 mg g^{-1} (nZVI-biochar) for MB, and 61.43 mg g^{-1} (biochar) and 83.13 mg g^{-1} (nZVI-biochar) for MG. The iron nanoparticle-loaded biochar exhibited higher adsorption capacities compared to the pristine biochar, indicating that the unmodified biochar was less effective in dye removal. The adsorption mechanisms were analyzed using the Langmuir, Freundlich, and Temkin isotherm models, and the corresponding adsorption capacities were calculated from these models. SEM analysis confirmed that the pyrolysis process provided the intended surface modification and generated a porous structure on the biochar. Elemental analysis revealed the presence of metal oxide nanoparticles in the biochar nanocomposite, verifying the success of the incorporation process. X-ray diffraction (XRD) analysis demonstrated that the raw biomass exhibited an amorphous structure, the biochar consisted of carbon and mineral components, and the nano-composite contained the intended iron nanoparticles. Overall, the findings indicate that both biochar and the nano-composite are highly promising materials for the treatment of contaminated water sources, particularly for efficient dye removal.

Scientific Ethics Declaration

* The authors declare that the scientific ethical and legal responsibility of this article published in EPSTEM journal belongs to the authors.

Conflict of Interest

* The authors declare that they have no conflicts of interest

Funding

* There is no funding

Acknowledgements or Notes

* This article was presented as an oral presentation at the International Conference on Technology, Engineering and Science (www.icontes.net) held in Antalya/Türkiye on November 12-15, 2025.

References

Baig, S. A., Zhu, J., Muhammad, N., Sheng, T., & Xu, X. (2014). Effect of synthesis methods on magnetic Kans grass biochar for enhanced As (III, V) adsorption from aqueous solutions. *Biomass and Bioenergy, 71*, 299-310.

Erdogan, F. O. (2017). Düşük maliyetli adsorbentler üzerine dispers sarı 211 tekstil boyasının adsorpsiyonu. *Afyon Kocatepe Üniversitesi Fen ve Mühendislik Bilimleri Dergisi, 17*(3), 889-898.

Erkmen, J., Kavcı, E., & Adıguzel, M. (2019). Üretim planlaması yapılarak su bazlı boyaların üretimi esnasında oluşan su kirliliğinin ve boya kaybının önlenmesi. *Journal of the Institute of Science and Technology, 9*(1), 57-65.

Erkus, A., Oygun, E., Turkmenoglu, M., & Aldemir, A. (2018). Boya endüstrisi atıksularının karakterizasyonu. *Yüzüncü Yıl Üniversitesi Fen Bilimleri Enstitüsü Dergisi, 23*(3), 308-319.

Gozeten, I., & Savran, A. (2018). Metil kırmızısının silikajel üzerindeki çözeltiden adsorpsiyonu: Denge izotermleri ve kinetik incelemeler. *Mus Alparslan University Journal of Science, 6*(2), 581-589.

Hung, C. M., Huang, C. P., Cheng, J. W., Chen, C. W., & Dong, C. D. (2021). Production and characterization of a high value-added seaweed-derived biochar: Optimization of pyrolysis conditions and evaluation for sediment treatment. *Journal of Analytical and Applied Pyrolysis, 155*, 105071.

Parlayıcı, S., & Pehlivan, E. (2017). Removal of metals by Fe3O4 loaded activated carbon prepared from plum stone (Prunus nigra): Kinetics and modelling study. *Powder Technology, 317*, 23-30.

Parlayıcı, S., & Pehlivan, E. (2021). Biosorption of methylene blue and malachite green on biodegradable magnetic Cortaderia selloana flower spikes: Modeling and equilibrium study. *International Journal of Phytoremediation, 23*(1), 26-40.

Parlayıcı, S., & Pehlivan, E. (2023). An ecologically sustainable specific method using new magnetic alginate-biochar from acorn cups (Quercus coccifera L.) for decolorization of dyes. *Polymer Bulletin, 80*(10), 11167-11191.

Rathi, B. S., Kumar, P. S., & Vo, D. V. N. (2021). Critical review on hazardous pollutants in water environment: Occurrence, monitoring, fate, removal technologies and risk assessment. *Science of the Total Environment, 797*, 149134.

Srivatsav, P., Bhargav, B. S., Shanmugasundaram, V., Arun, J., Gopinath, K. P., & Bhatnagar, A. (2020). Biochar as an eco-friendly and economical adsorbent for the removal of colorants (dyes) from aqueous environment: A review. *Water, 12*(12), 3561.

Yaseen, D. A., & Scholz, M. (2019). Textile dye wastewater characteristics and constituents of synthetic effluents: A critical review. *International Journal of Environmental Science and Technology, 16*(2), 1193-1226.

Yi, Y., Huang, Z., Lu, B., Xian, J., Tsang, E. P., Cheng, W., & Fang, Z. (2020). Magnetic biochar for environmental remediation: A review. *Bioresource Technology, 298*, 122468.

Author(s) Information

Erol Pehlivan
Konya Technical University, Faculty of Engineering and Natural Sciences, Department of Chemical Engineering Rauf Orbay Street. 42250, Selçuklu/Konya, Türkiye
Contact e-mail: *erolpehlivan@gmail.com*

Busra Ozkok
Konya Technical University, Faculty of Engineering and Natural Sciences, Department of Chemical Engineering, Rauf Orbay Street. 42250, Selçuklu/Konya, Türkiye

To cite this article:

Pehlivan, E. & Ozkok, B. (2025). Synthesis and characterization of biochar and nano-biochar composites derived from biomass (*Colutea cilicica*) for the removal of cationic dyes from aqueous solutions. *The Eurasia Proceedings of Science, Technology, Engineering and Mathematics (EPSTEM), 38,* 423-432.